References

[1]Prandtl, L., "Flüssigkeitsbewegung," *Handworterbuch der Naturwissenschaften*, Vol. 4, Gustav Fischer, Jena, Germany, 1913, pp. 101–140.

[2]Betz, A., "Untersuchungen von Tragflächen mit Verwundenen und nach Ruckwarts Gerichteten Enden," *Zeitschrift für Flugtechnik & Motorluftschiffahrt*, Vol. 5, 1914, pp. 16, 17.

[3]Prandtl, L., *Tragflächentheorie I. Mitteilung, Nachrichten der Gesellschaft der Wissenschaften zu Göttingen*, Mathematisch-Physikalisch Klasse, 1918, pp. 151–177.

[4]Lanchester, F. W., *Aerodynamics*, Constable and Co., London, 1907, pp. 139–178.

[5]van Dyke, M., *Perturbation Methods in Fluid Mechanics*, Parabolic Press, Stanford, CA, 1975, pp. 167–176.

[6]Saffman, P. G., *Vortex Dynamics*, Cambridge Univ. Press, Cambridge, England, U.K., 1992, pp. 95–115.

[7]Phillips, W. F., and Snyder, D. O., "Modern Adaptation of Prandtl's Classic Lifting-Line Theory," *Journal of Aircraft*, Vol. 37, No. 4, 2000, pp. 662–670.

[8]Glauert, H., *The Elements of Aerofoil and Airscrew Theory*, Cambridge Univ. Press, Cambridge, England, U.K., 1948, pp. 125–170.

[9]Phillips, J. D., "Downwash in the Plane of Symmetry of an Elliptically Loaded Wing," NASA-TP-2414, Jan. 1985.

A. Plotkin
Associate Editor

Assessment of Reaction Mechanisms for Counterflow Methane–Air Partially Premixed Flames

H. S. Xue* and S. K. Aggarwal[†]
University of Illinois at Chicago,
Chicago, Illinois 60607
R. J. Osborne[‡] and T. M. Brown[‡]
NASA Marshall Space Flight Center,
Huntsville, Alabama 35812
and
R. W. Pitz[§]
Vanderbilt University, Nashville, Tennessee 37325

Introduction

PARTIALLY premixed flames (PPF) are hybrid flames containing multiple reaction zones. These flames are of fundamental importance to the phenomena of nonpremixed flame stabilization and liftoff, spray combustion, and localized extinction and reignition in turbulent flames. A double flame containing a fuel-rich premixed reaction zone that synergistically interacts with a nonpremixed reaction zone is an example of a partially premixed flame. Because these flames are characterized by thermochemical interactions between the reaction zones that involve the transport of both stable and radical species, it is essential that the simulation of their structure employ a reliable and detailed chemistry model. Our previous investigation[1] of PPFs in a counterflow configuration focused on the capability of five different reaction mechanisms for predicting the detailed structure of methane–air PPF for

*Graduate Assistant, Department of Mechanical Engineering, 842 W. Taylor Street.
[†]Professor, Department of Mechanical Engineering. Associate Fellow AIAA.
[‡]Engineer.
[§]Professor and Head, Department of Mechanical Engineering. Member AIAA.

a range of strain rates and equivalence ratios. The reaction mechanisms included the C_1 and C_2 mechanisms of Peters, which were used in our previous investigation,[1] GRI-2.11 and GRI-3.0 mechanisms (data available online at http://www.me.berkeley.edu/gri-mech/ [cited 1 June 2001]), and a 12-step reduced mechanism.[2] The C_1 mechanism involves only C_1 species and 52 elementary reactions, whereas the C_2 mechanism considers both C_1 and C_2 species and involves 81 elementary reactions. The GRI-2.11 mechanism considers the chemistry of C_1- and C_2-species, involving 279 reactions and 49 species. The GRI-3.0 is the updated version of GRI-2.11 and involves 325 elementary reactions and 53 species. Differences between the two versions are outlined in on-line data at http://www.me.berkeley.edu/gri-mech/. The 12-step mechanism has been reduced from GRI-Mech 1.2 and validated by Sung et al.[2] for different combustion phenomena.

Results of our previous investigation[1] indicated that although all five mechanisms qualitatively reproduced the double-flame structure associated with PPFs there were significant quantitative differences between the flame structure obtained using the C_1 and C_2 mechanisms and that obtained using the GRI-2.11, GRI-3.0, and 12-step mechanisms. In particular, for low to moderate strain rates and high levels of air premixing ($\phi < 2.0$) the rich premixed reaction zone for the GRI-2.11, GRI-3.0, and 12-step mechanisms was located very close to the fuel nozzle and the physical separation between the two reaction zones was significantly larger compared to that for the C_1 and C_2 mechanisms. (Fuel nozzle here refers to the nozzle supplying the fuel-rich mixture. Also, the axial distance for presenting the computed and measured profiles in the present Note is measured from the fuel nozzle.) A lack of experimental data precluded making any definite conclusions as to which mechanism provided a more realistic prediction of the partially premixed flame structure. In the present investigation we employ experimental data of Osborne[3] to further examine and validate these mechanisms. Because there were not significant differences between the predictions of C_1 and C_2 mechanisms and between the predictions of GRI-2.11, GRI-3.0, and 12-step mechanisms, we focus here on validating the C_2 and GRI-3.0 mechanisms.

Results and Discussion

The counterflow methane–air partially premixed flame was computed using the Oppdif[4] and Chemkin[5] packages. Details regarding these packages can be found elsewhere.[1,4,5] An optically thin radiation model was incorporated into the original code to account for the radiation heat loss. Details are provided elsewhere.[1]

Measurements

Nonintrusive laser diagnostics are used to study methane–air partially premixed flames in a counterflow burner.[6] The burner is based on a previous design by Trees et al.[7] A similar configuration has also been developed by Mastorakos et al.[8] to examine the extinction behavior of turbulent counterflow flames. Measurements of species, including CH_4, CO_2, CO, O_2, N_2, and H_2O, and temperature are made axially from the exit of the methane–air jet, through the flame zone, to the exit of the airjet with spontaneous Raman scattering induced by a 20-ns laser shot from a narrowband tunable KrF excimer laser (200 mJ at 248 nm). The laser beam is focused by a 2-m lens to a 0.7×0.3 mm cross section in the measurement volume. Spontaneous Raman-scattered light from CH_4, CO_2, CO, O_2, N_2, and H_2O molecules is collected by $f/1.5$ Cassegrain optics and focused onto the entrance slit of a $\frac{1}{2}$-m Spex spectrometer. The spectrometer entrance slit collects light from a 0.2-mm length of the laser beam. Thus, the measurement volume is $0.7 \times 0.3 \times 0.2$ mm. The spectrometer spectrally separates the light and focuses the diffracted images of the slit onto a Princeton Instruments intensified charge-coupled device.

Measurements of the opposed flow flame are made by applying the calibrated Raman system to the counterflow burner. Flames with equivalence ratio of 1.4 and strain rates of 100, 150, and 200 s^{-1} are measured. Data sets, each containing 310 shots, are recorded and averaged for consecutive positions along the axial dimension (stagnation streamline) of the burner. The spatial resolution along the stagnation streamline is 0.3 mm. The UV Raman setup, calibration

Table 1 Error estimates

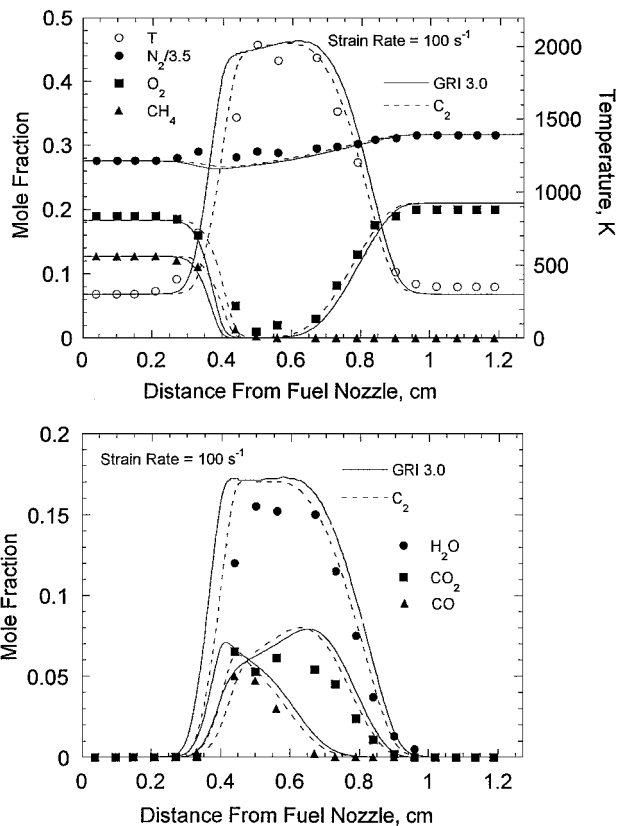| Species	Statistical error, %	Calibration error, %
CO_2	2.5	7
O_2	1	5
CO	2	10
N_2	1	2
CH_4	1	2
H_2O	2	2
T	1	7

Fig. 1 Comparison of the predicted and measured flame structures in terms of temperature and major species mole fraction profiles for a partially premixed flame (PPF) established at a strain rate of $100 \ \text{s}^{-1}$ and equivalence ratio of 1.4.

procedure, and data corrections are described in more detail by Osborne.[3]

The data averaged over 310 shots yield mean measurements in which the statistical errors are small relative to the systematic errors. These systematic errors are caused by limited calibration data and various other sources. In accessing the precision of the Raman system, the shot-to-shot variation (or the relative standard deviation) of the Raman signals used in the system calibration ranged from 5% for N_2 up to 40% for CO_2. However, the standard error of the mean measurements was much smaller as a result of the number of shots collected. Therefore, the overall statistical error in the mean was no more than 2.5% for the minor species. Calibration errors resulting from errors in curve fits and signal cross talk were, in general, larger than the statistical errors. Other absolute errors in the Raman measurements were caused by polycyclic aromatic hydrocarbon (PAH) interferences, incorrect background light subtraction, and laser energy measurement errors. Table 1 indicates estimates of statistical and calibration errors.

Comparison

Figure 1 presents a comparison of the predicted and measured structures of a methane–air partially premixed flame in terms of the temperature and major species mole fraction profiles. The equivalence ratio ϕ of the fuel stream is 1.4, and the fuel and airjet
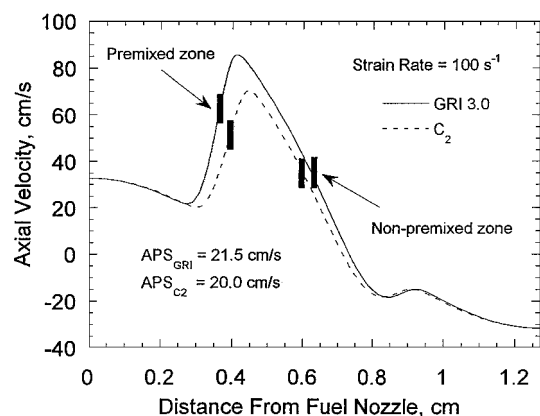
velocities at the respective nozzle exits are 32.7 and 31.6 cm/s. Using the equation[6]

$$a_s = \frac{2|v_0|}{L}\left(1 + \frac{|v_f|\sqrt{\rho_f}}{|v_o|\sqrt{\rho_o}}\right) \qquad (1)$$

the strain rate for this case is $100 \ \text{s}^{-1}$ in both experiments and simulations, where $L = 1.27 \ \text{cm}$. The measured boundary conditions are used for the simulations.

The predicted flame structure for both the C_2 and GRI-3.0 mechanisms shows excellent qualitative agreement with measurements. However, the quantitative agreement with the measured data seems to be better when C_2 mechanism is employed. The GRI-3.0 mechanism predicts a relatively wider flame (that is, the two reaction zones are spatially more separated) compared to experiments as well as predictions using the C_2 mechanism. This is consistent with the observations made in our earlier investigation regarding the comparison of GRI-3.0 and C_2-mechanisms. Also our previous study[1] indicated that at low strain rates ($a_s = 19.7 \ \text{s}^{-1}$) the GRI-2.11 mechanism yields a flame that is wider than that obtained using the GRI-3.0 mechanism. Consequently, the GRI-3.0 mechanism represents an improvement over the GRI-2.11 mechanism in modeling PPFs. Both the C_2 and GRI-3.0 mechanisms overpredict the concentration of major product species, namely H_2O, CO_2, and CO, compared to measurements, implying some experimental uncertainty in the measurements of these species.

Figure 2 presents axial velocity profiles for the flame of Fig. 1 obtained using GRI-3.0 and C_2 mechanisms. The locations of the rich premixed and nonpremixed reaction zones are marked by two black bars. In our previous study[1] it was shown that the lowest axial velocity upstream of the premixed reaction zone, which was termed as the apparent premixed flame speed (APS), could be used to characterize partially premixed flames. From Fig. 2 the computed values of APS for the GRI-3.0 and C_2 flames are 21.5 and 20.7 cm/s, respectively.

In Figs. 3 and 4 the computed flame structure obtained by using the GRI 3.0 and C_2 mechanisms is compared with measurements at higher strain rates (for example, $a_s = 150$ and $200 \ \text{s}^{-1}$). Although there is still good qualitative agreement between the predicted and measured profiles, the degree of agreement deteriorates at higher strain rates. For $a_s = 150 \ \text{s}^{-1}$ the nonpremixed branch of the partially premixed flame exhibits good agreement, whereas the rich premixed branch shows discrepancies between the predictions and measurements. The predicted temperature and species profiles have steeper gradients compared to the measured profiles in the rich premixed branch. The agreement between the predictions and measurements further deteriorates at $a_s = 200 \ \text{s}^{-1}$. The measured values of the peak temperature and H_2O mole fraction are significantly lower compared to the predicted values, even though there is good agreement between the measured and predicted peak values of CO_2 and CO mole fractions. The experimentally measured flame seems to be approaching extinction at $a = 200 \ \text{s}^{-1}$ with reduced flame temperature, reduced H_2O mole fraction, and increased oxygen leakage. The simulations do not show this trend at this strain rate. However, limited data calibration as well as PAH fluorescence interferences

Fig. 2 Axial velocity profiles for a PPF, computed using the GRI-3.0 and C_2 mechanisms, corresponding to the conditions of Fig. 1.
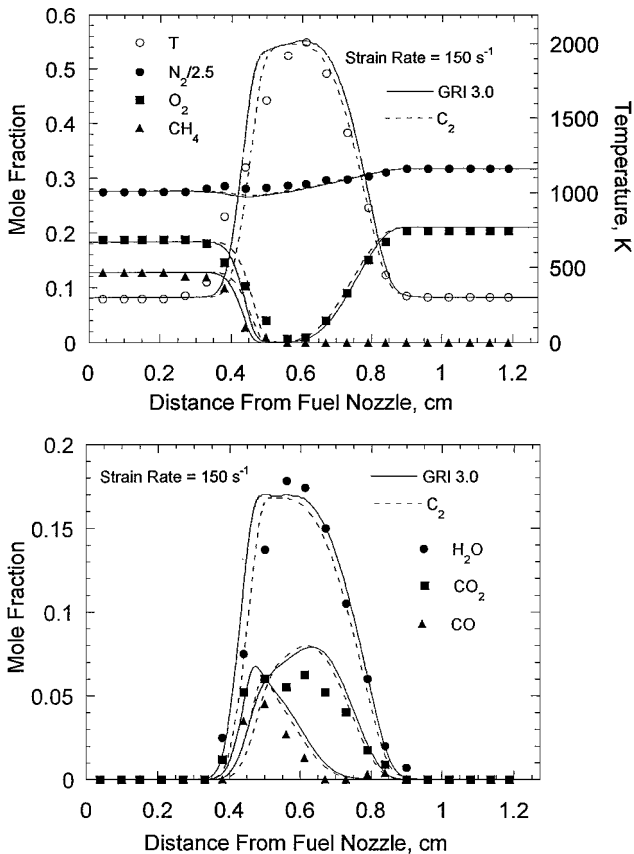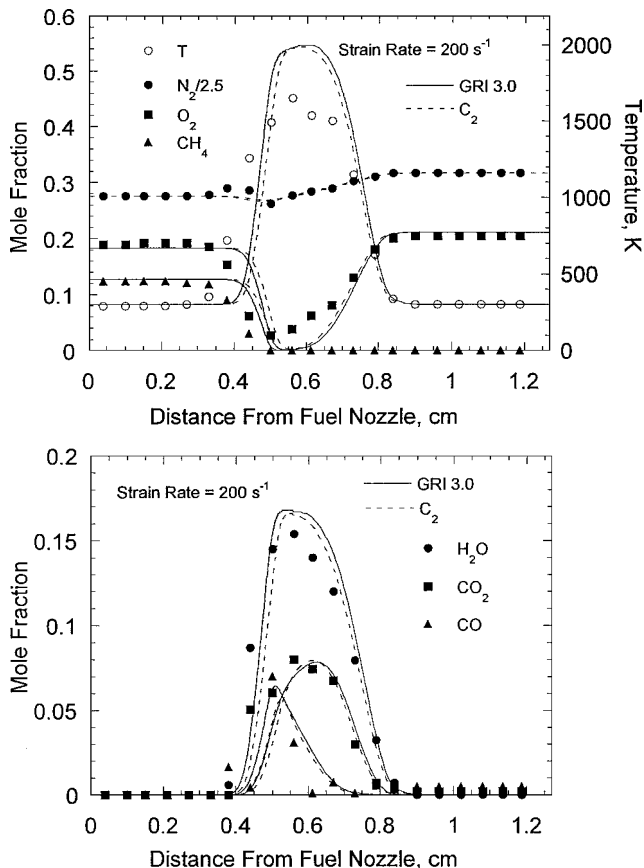
Fig. 3 Comparison of the predicted and measured flame structures in terms of temperature and species mole fraction profiles for a PPF established at a strain rate of 150 s⁻¹ and equivalence ratio of 1.4.

Fig. 4 Comparison of the predicted and measured flame structures in terms of temperature and species mole fraction profiles for a PPF established at a strain rate of 200 s⁻¹ and equivalence ratio of 1.4.

might have produced inconsistent results in the experimental data, especially in the rich premixed flame zones where PAH concentrations are the highest. A relatively large measurement resolution (0.3 mm) might also have contributed to the measurement errors.

Conclusions

The detailed measurements have been used to examine the applicability of GRI-3.0 and C_2 mechanisms for predicting the structure of methane–air partially premixed flames. The measured and predicted profiles of temperature and major species mole fractions have been compared for PPFs established at an equivalence ratio of 1.4 and strain rates of 100, 150, and 200 s⁻¹. For $a_s = 100$ s⁻¹ predictions for both the C_2 and GRI-3.0 mechanisms show excellent qualitative agreement with measurements. The quantitative agreement between predictions and experiments is better using the C_2 mechanism. The GRI-3.0 mechanism predicts a relatively wider flame compared to experiments as well as predictions based on the C_2 mechanism. This is consistent with the observations made in our earlier investigation[1] regarding the comparison of GRI-3.0 and C_2 mechanisms.

At higher strain rates ($a_s = 150$ and 200 s⁻¹) the quality of agreement between the measured and predicted data deteriorates. Because the flame structures predicted by using the C_2 and GRI-3.0 mechanisms show good agreement, there are perhaps greater inaccuracies in measurements at high strain rates.

GRI-3.0 and C_2 mechanisms exhibit differences in the prediction of partially premixed flames, although they show excellent agreement in predicting the premixed flame speeds,[1] the flammability limits, and the nonpremixed flame structure.[1] This implies that a partially premixed flame can provide a more rigorous test bed for the validation of detailed reaction mechanisms. More extensive experimental data are needed to validate mechanisms for PPFs.

References

[1]Xue, H., and Aggarwal, S. K., "Effects of Reaction Mechanisms on the Structure and Extinction of Partially Premixed Counterflow Flames," *AIAA Journal*, Vol. 39, No. 4, 2001, pp. 637–645.

[2]Sung, C. J., Law, C. K., and Chen, J.-Y., "An Augmented Reduced Mechanism for Methane Oxidation with Comprehensive Global Parametric Validation," *Proceedings of the Combustion Institute*, Vol. 27, 1998, pp. 295–304.

[3]Osborne, R. J., "Application of Ultraviolet Raman Spectroscopy to Methane-Air vs. Air Counterflow Flames," M.S. Thesis, Dept. of Mechanical Engineering, Vanderbilt Univ., Nashville, TN, March 1999.

[4]Lutz, A. E., Kee, R. J., Grcar, J. F., and Rupley, F. M., "OPPDIF: A Fortran Program For Computing Opposed-Flow Diffusion Flames," Sandia Labs., Rept. 96-8243, Albuquerque, NM, May 1997.

[5]Kee, R. J., Rupley, F. M., and Miller, J. A., "Chemkin: A Fortran Chemical Kinetics Package for the Analysis of Gas Phase Chemical Kinetics," Sandia Labs., Rept. 89-8009B, Albuquerque, NM, Jan. 1993.

[6]Tanoff, M. A., Smooke, M. D., Osborne, R. J., Brown, T. M., and Pitz, R. W., "The Sensitive Structure of Partially Premixed Methane-Air vs. Air Counterflow Flames," *Proceedings of the Combustion Institute*, Vol. 26, 1996, pp. 1121–1128.

[7]Trees, D., Brown, T. M., Smooke, M. D., Seshadri, K., Balakrishnan, G., Pitz, R. W., Giovangigli, V., and Nandula, S. P., "The Structure of Nonpremixed Hydrogen-Air Flames," *Combustion Science and Technology*, Vol. 104, 1995, pp. 427–439.

[8]Mastorakos, E., Taylor, A. M. P., and Whitelaw, J. H., *Combustion and Flame*, Vol. 91, No. 1, 1992, pp. 40–54.

I. Gokalp
Associate Editor